

Phase diagram of ferroelectrics with tricritical and Lifshitz points at coupling between polar and antipolar fluctuations

V. Liubachko,¹ A. Oleaga,² A. Salazar,² R. Yevych,¹ A. Kohutych,¹ and Yu. Vysochanskii¹

¹*Institute for Solid State Physics and Chemistry,*

Uzhgorod University, Pidgirna Str. 46, Uzhgorod, 88000, Ukraine

²*Departamento de Física Aplicada I, Escuela de Ingeniería de Bilbao,*

Universidad del País Vasco UPV/EHU, Plaza Torres Quevedo 1, 48013, Bilbao, Spain

(Dated: January 1, 2020)

Static and dynamic critical behavior of $\text{Sn}_2\text{P}_2\text{S}_6$ type ferroelectrics and $(\text{Pb}_y\text{Sn}_{1-y})_2\text{P}_2(\text{Se}_x\text{S}_{1-x})_6$ mixed crystals with line of tricritical points and line of Lifshitz points on the $T-x-y$ phase diagram, which meet at the tricritical Lifshitz point, can be described in a combined BEG-ANNNI model. Such the model considers first and second neighbor interactions for pseudospins in a local three-well potential. Below the temperature of tricritical Lifshitz point, the “chaotic” state accompanied by the coexistence of ferroelectric, metastable paraelectric and modulated phases is expected. In addition to the frustration of polar fluctuations near the Brillouin zone center, in $\text{Sn}_2\text{P}_2\text{S}_6$ crystal the antipolar fluctuations also strongly develop in the paraelectric phase at cooling to continuous phase transition temperature T_0 . Here, critical behavior can be described as a crossover between Ising and XY universality classes, what is expected near bicritical points with coupled polar and antipolar order parameters and competing instabilities in q -space.

PACS numbers: 64.60.Kw, 64.60.Fr, 77.80.-e, 77.80.Bh

I. INTRODUCTION

Competing order parameters produce rich phase diagrams of crystals with dipolar ordering in terms of temperature vs external fields, pressure and doping.¹ Besides, existence of competing ferroelectric, incommensurately modulated and antiferroelectric states with different symmetries in the ground state of the system can be observed. The usual approach to describe the phase diagrams is the Landau-Ginzburg expansion of the free energy density in terms of the order parameters.² At microscopic level, the phase diagrams can be obtained by using mean-field approximations of simplified model Hamiltonians.³ At any consideration the main qualitative properties of the phase diagram are determined by investigated system symmetry.

The active role of several types of mode-mode couplings also is reflected in the complex shape of the local potential for spontaneous polarization fluctuations. It determines the appearance of phase diagrams with different multicritical points that have been intensively studied in the case of oxide materials.⁴⁻⁷ The chalcogenide ferroelectrics of $\text{Sn}_2\text{P}_2\text{S}_6$ family also present a rich set of scenarios for critical behavior realization^{8,9} and comparison with the theoretical investigations.^{10,11}

Ferroelectrics of the $\text{Sn}_2\text{P}_2\text{S}_6$ family are promising candidates for application in red and near-infrared spectral diapason photorefraction¹² and photovoltaics,¹³ for energy storage¹⁴ and low temperature thermometry,^{15,16} as well as development of multilevel-cell-type memory technology.¹⁷ Possibilities of ultrafast spontaneous polarization switching¹⁸ and peculiarities in the ferroelectric ordering and domain structure morphology at nanoscale^{19,20} are also important for new technologies based on ferroics with linear and nonlinear coupling be-

tween unstable lattice polar modes and antipolar or antiferrodistorsive degrees of freedom.

In $\text{Sn}_2\text{P}_2\text{S}_6$ crystals the second order phase transition at $T_0 \approx 337$ K with lattice symmetry lowering from $P2_1/c$ to Pc has mixed displacive-order/disorder character^{21,22} which is manifested by high values of both the transition entropy²³ $\Delta S = 8.6 \text{ JK}^{-1}\text{mol}^{-1}$ and the dielectric anomaly of the Curie-Weiss constant²⁴ $C \approx 10^5$ K. In $\text{Sn}_2\text{P}_2\text{S}_6$ crystals under compression, the second order transitions line $T_0(p)$ is monotonously decreases with increasing of temperature and after reaching the tricritical point (TCP) at $p_{\text{TCP}} \approx 0.6$ GPa and $T_{\text{TCP}} \approx 220$ K, it becomes first order.^{25,26} At Sn by Pb replacement in $(\text{Pb}_y\text{Sn}_{1-y})_2\text{P}_2\text{S}_6$ solid solutions the continuous phase transitions line $T_0(y)$ becomes first order at $y \geq y_{\text{TCP}} \approx 0.2$ and $T \leq T_{\text{TCP}} \approx 220$ K, and the paraelectric phase becomes stable at cooling down to 0 K for $y \geq 0.6$.^{27,28} At sulfur by selenium substitution in $\text{Sn}_2\text{P}_2(\text{Se}_x\text{S}_{1-x})_6$ mixed crystals, the incommensurate (IC) phase appears for $x \geq x_{\text{LP}} \approx 0.28$ (where x_{LP} is the concentration at which the Lifshitz point (LP) appears) on the temperature-concentration diagram.⁹ The virtual paraelectric-ferroelectric transition (inside the IC phase) becomes first order at $x \geq x_{\text{VTCP}} \approx 0.6$ and $T \leq T_{\text{VTCP}} \approx 220$ K.⁸

It is seen that under any influence, that lowers the ferroelectric phase transition temperature below 220 K, transition character evolves to first order, what has been explained within a model with three-well local potential for the spontaneous polarization fluctuations.²⁹ Such shape of the potential energy landscape in $\text{Sn}_2\text{P}_2\text{S}_6$ ferroelectrics can be described on the basis of a second order Jahn-Teller effect with nonlinear coupling of polar (B_u -symmetry) and fully symmetrical (A_g -symmetry) long wave fluctuations. This local potential was found

by first principles calculations³⁰ and is related to $5s^2$ electrons lone pair stereoactivity of Sn^{2+} cations.^{30,31} The charge disproportionation of phosphorous cations $P^{3+} + P^{5+} \leftrightarrow P^{4+} + P^{4+}$ also originates an electronic contribution to the spontaneous polarization.²⁹ The evolution of pseudospin distribution in three-well local potential while decreasing the temperature was found by MC simulations,³⁰ and it is comparable with experimental data of ^{31}P NMR spectroscopy.³²

In addition to the microscopic atomistic consideration, the nature of the phase transition in $\text{Sn}_2\text{P}_2\text{S}_6$ crystals was also analyzed within the framework of the thermodynamic three-state Blume-Emery-Griffith (BEG) model^{33,34} that supposes 0, +1 and -1 values for local pseudospins and predicts the TCP presence on a temperature-pressure or temperature-composition phase diagram of mixed crystals. The TCP presence and the lowering of the phase transition temperature till 0 K are determined by pressure or composition evolution of the local three-well potential shape (change of the energy difference between central and side wells) and was analyzed in the approach of the quantum anharmonic oscillators (QAO) model for $\text{Sn}_2\text{P}_2\text{S}_6$ crystals.²⁹ The calculated spectra of pseudospin fluctuations in the framework of the QAO model correlate well with the observed Raman spectra transformation in the ferroelectric phase with appearance of low-energy modes.³⁵ Besides, the $\text{Sn}_2\text{P}_2\text{S}_6$ crystal lattice anharmonicity on example of thermal expansion temperature anomaly was successfully described using the QAO model.³⁶

The appearance of the IC phase in $\text{Sn}_2\text{P}_2\text{S}_6$ family crystals can be explained using the discrete axial Ising model — ANNNI model,³⁷ that consider short range interaction $J_1 > 0$ between the nearest neighbors, and interaction $J_2 < 0$ between next-nearest neighbors. The ratio of these interactions $\lambda = -J_2/J_1$ changes at sulfur by selenium substitution in $\text{Sn}_2\text{P}_2(\text{Se}_x\text{S}_{1-x})_6$ mixed crystals — the IC phase appears at the LP with coordinate $\lambda = 0.25$. It was estimated²⁴ that λ changes from 0.23 for composition with $x = 0$ to 0.3 for $x = 1$.

Discrete ANNNI model introduces into consideration two sublattices of $\text{Sn}_2\text{P}_2\text{S}_6$ type crystals structure with two formula units in the elementary cell. They were involved in the description of the IC phase, for which the wave vector of the spontaneous polarization transverse space modulation wave lies on the monoclinic symmetry plane near [001] direction.²⁴ The spontaneous polarization vector also lies in the monoclinic symmetry plane (010) and oriented near [100] direction. Experimental data of neutron scattering for $\text{Sn}_2\text{P}_2\text{S}_6$ crystal demonstrate flexoelectric coupling between soft optical and acoustic phonon branches near the Brillouin zone center as their repulsion due to the same symmetry along q_z direction of reciprocal space.³⁸ This coupling has also been observed in temperature anomalies of ultrasound and hypersound velocity.³⁹ In the continuous approximation, the linear flexoelectric interaction between optical and acoustic phonons is related to the

Lifshitz like invariant $(dP_x/dz)u_{xz}$ in the thermodynamic potential.^{40,41} Its growth at crossing from $\text{Sn}_2\text{P}_2\text{S}_6$ to $\text{Sn}_2\text{P}_2\text{Se}_6$ causes by a higher covalence of chemical bonds in selenide compound.⁴²

The neutron scattering data⁴³ also show the presence of a flat lowest-energy transverse optical branch along q_y direction in the paraelectric phase of $\text{Sn}_2\text{P}_2\text{S}_6$ crystal. Developed diffuse X-ray scattering along q_y direction in the paraelectric phase near temperature T_0 also confirms an important role of the possibility of short-wave antipolar fluctuations.⁴⁴

In this paper we use the model approaches for the description of the phase diagram topology of $\text{Sn}_2\text{P}_2\text{S}_6$ based ferroelectric mixed crystals as well as of the critical behavior of their thermodynamic and dynamic properties, considering the important role of developed polar fluctuations coupling with fully symmetrical and antipolar fluctuations together with frustrations whenever there is a competition between different instabilities in reciprocal q -space.

II. PHASE DIAGRAM WITH TRICRITICAL LIFSHITZ POINT

In order to build the $T - \lambda - \Delta$ phase diagram for ferroelectrics in the system $\text{Sn}(\text{Pb})_2\text{P}_2\text{S}(\text{Se})_6$, we have used the Blume-Capel spin-1 Ising model (which is a simpler version of BEG model) with competing interactions.^{45,46} Such combined BC-ANNNI model displays a multicritical behavior such as tricriticality as well as the possibility of the presence of a LP. The tricritical Lifshitz point (TCLP) is predicted at the meeting of TCPs and LPs lines.⁴⁷⁻⁴⁹ In the used model⁴⁵ (as for original ANNNI model³⁷) the relation between two interactions is written in the form $\lambda = -J_2/J_1$, where J_1 is the effective first neighbors positive interaction and J_2 is the negative coupling of next nearest neighbors. The paraelectric-ferroelectric second order transitions line can be found as⁴⁵

$$\lambda = 1 - \frac{t}{1 + 0.5e^{\Delta/t}} \quad (1)$$

and from the paraelectric phase into a modulated one continuous transitions line

$$\lambda = \frac{t}{1 + 0.5e^{\Delta/t}}. \quad (2)$$

Here $t = T/J_1$, and $\Delta = \delta/J_1$. The parameter δ is related to the single-ion terms.^{29,33} At $\lambda = 0.25$ the paraelectric borders obtained from (1) and (2) meet at a LP. Considering the above-mentioned conditions, the line of LPs can be found by means of the following equation

$$\Delta = t_{\text{LP}} \ln \frac{1 - 2t_{\text{LP}}}{t_{\text{LP}}}. \quad (3)$$

After reaching a value $\Delta \approx 0.231$ the paraelectric borders begin to split and there is no LP anymore. Near

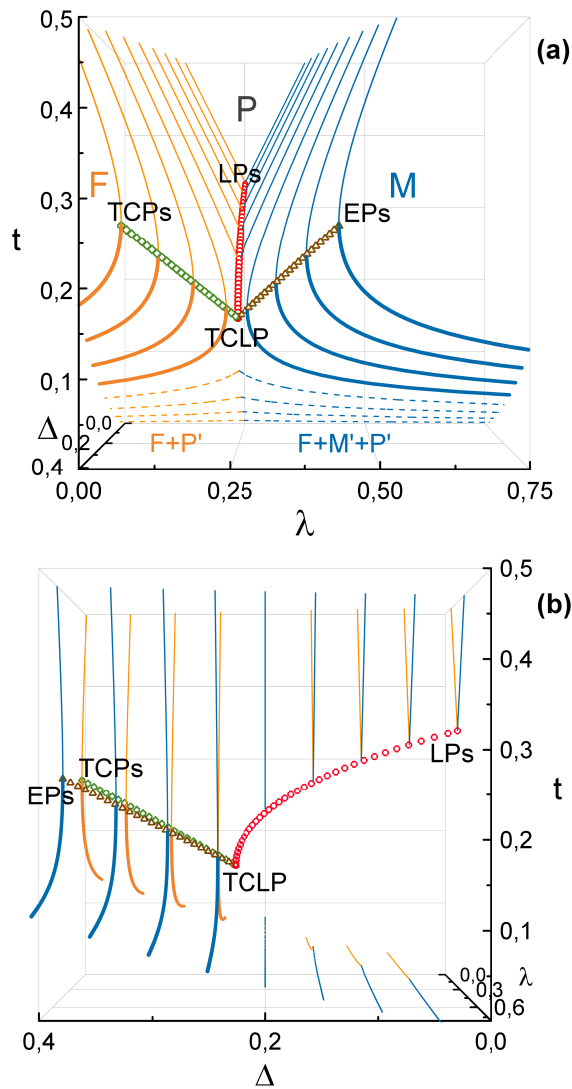


FIG. 1. (a) Front and (b) side view on calculated $t - \lambda - \Delta$ diagram. Solid lines show paraelectric-ferroelectric (orange) and paraelectric-modulated (blue) borders, Lifshitz points (LPs) line (red circles), tricritical points (TCPs) line (green squares), end points (EPs) line (brown triangles). Thin lines indicate the second order phase transitions while thick lines are the first order ones. Letters F, P and M correspond to ferroelectric, paraelectric and modulated phases. The coexistence of ferroelectric and metastable paraelectric (F+P') and ferroelectric, metastable paraelectric and commensurate modulated phases (F+M'+P') below the dashed lines are also shown.

this Δ value the LPs line coincides with the TCPs line and the end points line.⁴⁵ The calculated $t - \lambda - \Delta$ phase diagram is depicted in Fig. 1.

Lets compare the just obtained theoretical phase diagram with the experimentally determined temperature-concentration phase diagram for $(\text{Pb}_y\text{Sn}_{1-y})_2\text{P}_2(\text{Se}_x\text{S}_{1-x})_6$ ferroelectric mixed crystals.²⁴ In order to do it we need to translate it into $t - \lambda - \Delta$

coordinates. The experimentally observed⁵⁰ TCLP for $(\text{Pb}_{0.05}\text{Sn}_{0.95})_2\text{P}_2(\text{Se}_{0.28}\text{S}_{0.72})_6$ at $T_{\text{TCLP}} \approx 259$ K in $t - \lambda - \Delta$ coordinates will correspond to the next position: $t = 0.158249$, $\lambda = 0.5$, $\Delta = 0.23105$. The LP with the composition $\text{Sn}_2\text{P}_2(\text{Se}_{0.28}\text{S}_{0.72})_6$ at temperature $T_{\text{LP}} \approx 284$ K (Ref. 9) will lie on the line of LPs obtained from eq. (3) at $t = 0.17345$, $\lambda = 0.5$, $\Delta = 0.22997$. For mixed $\text{Sn}_2\text{P}_2(\text{Se}_x\text{S}_{1-x})_6$ crystals in the framework of the ANNNI model, a linear variation of the λ parameter with composition x was assumed with the values 0.23, 0.25 and 0.30 for $\text{Sn}_2\text{P}_2\text{S}_6$, $\text{Sn}_2\text{P}_2(\text{Se}_{0.28}\text{S}_{0.72})_6$ and $\text{Sn}_2\text{P}_2\text{Se}_6$, respectively.²⁴ At the constant value $\Delta = 0.22997$, the coordinates for these concentrations on the $t - \lambda - \Delta$ diagram are the following: $t_0 = 0.20582$, $\lambda = 0.23$ for $\text{Sn}_2\text{P}_2\text{S}_6$ with $T_0 = 337$ K; $t_c = 0.13436$, $\lambda_c = 0.30$, and $t_i = 0.11799$, $\lambda_i = 0.30$ for $\text{Sn}_2\text{P}_2\text{Se}_6$ with $T_c = 220$ K, and $T_i = 193$ K.²⁴

At tin by lead substitution the shape of local three-well potential changes, and the coordinates of the TCP in the $(\text{Pb}_y\text{Sn}_{1-y})_2\text{P}_2\text{S}_6$ mixed crystals in mean-field approximation of BEG model⁵¹ can be determined at condition of linear variation of Δ in dependence of y , at unchanged intercell interactions. According to the earlier performed analysis for $(\text{Pb}_y\text{Sn}_{1-y})_2\text{P}_2\text{S}_6$ mixed crystals,²⁹ the calculated $t - \Delta$ diagram (at $\lambda = 0.23$) is shown in Fig. 2. It was found that the TCP has coordinates $\lambda = 0.23$, $t = 0.13436$, $\Delta = 0.23577$.

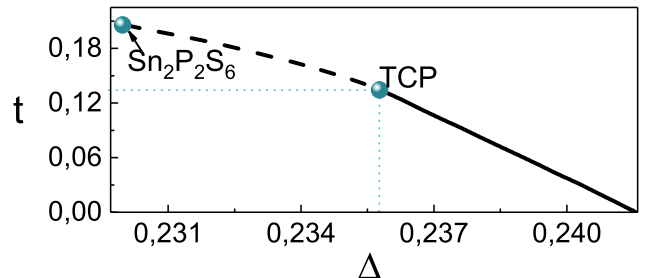


FIG. 2. Dependence of phase transition temperature on the single-ion term in dimensionless $t - \Delta$ coordinates calculated in the mean-field approximation on the BEG model.^{29,51} Dashed and solid lines indicate second and first order transitions, respectively, that meet at the tricritical point.

As the inter-site interaction J_1 is an almost unchanged quantity,²⁹ we assume that, on increasing the lead concentration in $(\text{Pb}_y\text{Sn}_{1-y})_2\text{P}_2\text{Se}_6$ mixed crystals (with $\lambda = 0.3$), the value of Δ will change in the same way as in $(\text{Pb}_y\text{Sn}_{1-y})_2\text{P}_2\text{S}_6$ solid solutions. Accordingly, the experimental phase diagram in $t - \lambda - \Delta$ coordinates is presented in Fig. 3.

From the calculated $t - \lambda - \Delta$ diagram, it follows that the LPs line terminates at TCLP, and this multicritical point can be considered as a Lifshitz end point. The LPs line in TCLP splits into the tricritical points line and the end points line. At big Δ parameter, the paraelectric-modulated critical line ends at the end point.⁴⁵

For high lead concentrations ($y > 0.2$), at low

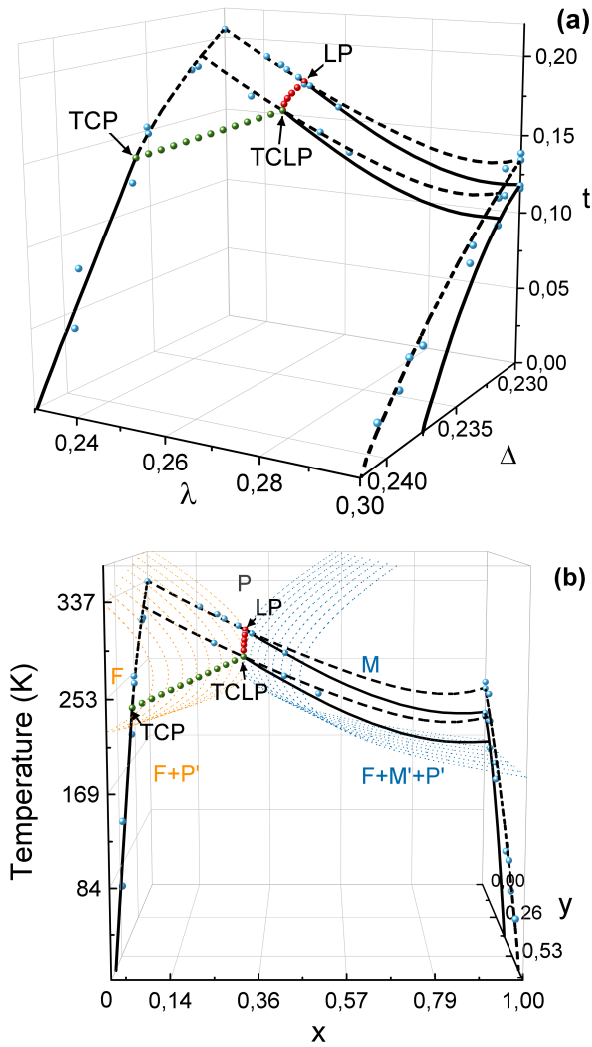


FIG. 3. (a) Experimental phase diagram in $t - \lambda - \Delta$ coordinates for $(\text{Pb}_y\text{Sn}_{1-y})_2\text{P}_2(\text{Se}_x\text{S}_{1-x})_6$ ferroelectrics and (b) front view of both experimental and calculated phase diagrams in temperature-concentration $T - x - y$ coordinates. Dashed and solid lines denote second order and first order phase transitions, respectively. Green and red spheres correspond to tricritical points line and Lifshitz points line, blue spheres to the calorimetric data.^{28,50,52–56}

temperatures a chaotic state can be observed.⁴⁵ This state presents a mixture of paraelectric, ferroelectric and modulated phases. Such peculiarity can be seen on the excess heat capacity ΔC_p and anomalous temperature dependencies of dielectric susceptibility ϵ' in $(\text{Pb}_y\text{Sn}_{1-y})_2\text{P}_2\text{Se}_6$ crystals, according to recent investigations.^{15,16,57,58} For small lead concentrations, there are clear anomalies of $\Delta C_p(T)$ and $\epsilon'(T)$ at paraelectric-incommensurate (T_i) and incommensurate-ferroelectric (T_c) phase transitions (see Fig. 4, 5). However, for $y \geq 0.2$ the $\Delta C_p(T)$ and $\epsilon'(T)$ anomalies in the vicinity of the lock-in transition (T_c) are strongly smeared. Such chaoticization can be related to a synergy of frustration effects and nonlinearity of the system with

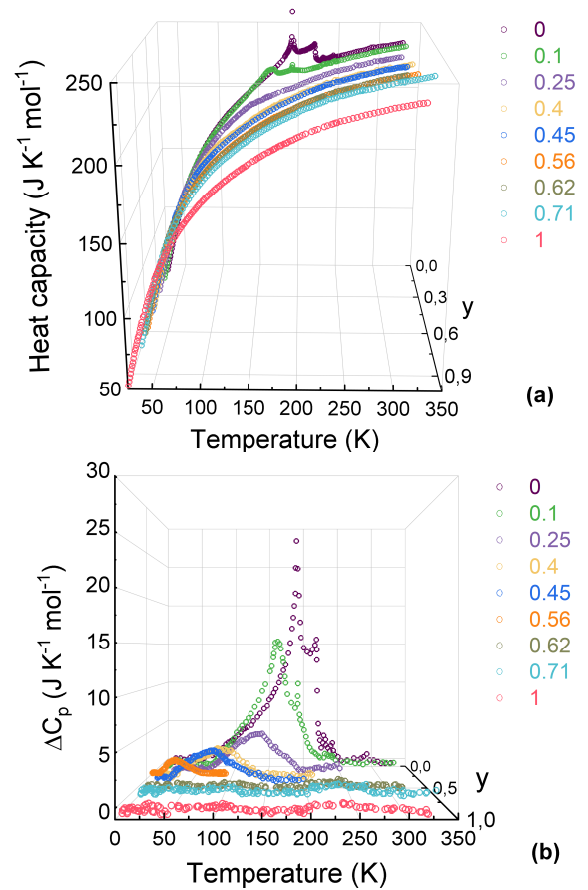


FIG. 4. Temperature dependence of (a) heat capacity according to experimental data⁵⁷ and (b) related to the phase transition excess heat capacity for $(\text{Pb}_y\text{Sn}_{1-y})_2\text{P}_2\text{Se}_6$ crystals.

the three-well local potential.

Therefore, the ANNNI model with two structural sublattices reflects the main properties of ferroelectrics that are related to the LP and IC phase on their phase diagram. For the description of a presence of a TCP on the phase diagram of $\text{Sn}_2\text{P}_2\text{S}_6$ family ferroelectrics, two structural sublattices were also considered in the frame of BEG model.^{33,34} This three-state model is based on two order parameters — dipolar and quadrupolar (B_u and A_g symmetry variables in the case of $\text{Sn}_2\text{P}_2\text{S}_6$).^{30,31} Therefore, in addition to dipole-dipole inter-site coupling, the quadrupole-quadrupole interaction can also be important. In the case of two sublattices, taking into account the quadrupole-quadrupole interactions can complicate the topology of the temperature-pressure (composition) phase diagram. On such diagram, in addition to (or instead of) the presence of a TCP, another multicritical points can appear, such as a triple point, a critical end point, a bicritical point, and a tetracritical point.³⁴ In the case of negative quadrupole-quadrupole coupling at temperature lowering, in addition to the ferroelectric state, ferroelectric and antiquadrupolar phases can also appear.³⁴ With growth of positive quadrupole-

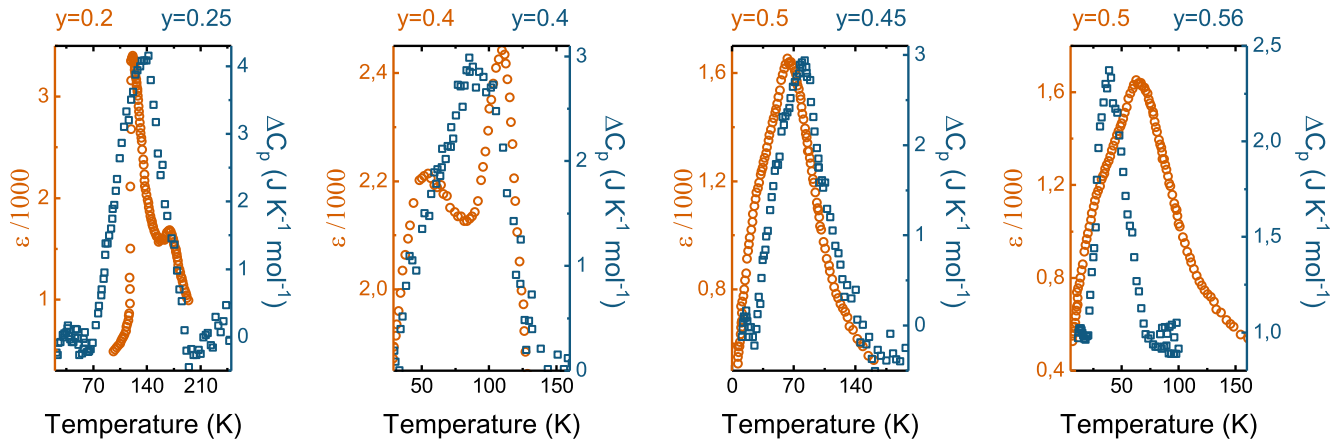


FIG. 5. Comparison of the anomalies for low frequency dielectric susceptibility (according to data^{15,16,58}) and excess heat capacity (according to data⁵⁷) in the region of the phase transitions for $(\text{Pb}_y\text{Sn}_{1-y})_2\text{P}_2\text{S}_6$ crystals.

quadrupole coupling, this TCP transforms into a triple point. In such case, at cooling in the paraelectric phase the first order transition with change of quadrupolar order parameter occurs, and with further temperature lowering the second order transition into ferroelectric state is observed.³⁴

III. POLAR AND ANTIPOLAR FLUCTUATIONS COUPLING

The above mentioned examples of possible complications of experimentally observed phase diagrams for objects with complex local potential for spontaneous polarization fluctuations demonstrate the proximity of the phase transitions to higher order multicritical points, like a tetracritical point, and give evidence of the importance of higher order invariants in the thermodynamic potential of the investigated ferroelectric crystals. Such possibility was earlier demonstrated^{59,60} when the incommensurate phase properties near lock-in transition into the ferroelectric phase in $\text{Sn}_2\text{P}_2\text{S}_6$ crystals were theoretically explained.

For $\text{Sn}_2\text{P}_2\text{S}_6$ ferroelectrics, the experimental data of neutron scattering, dielectric susceptibility and hysteresis loops investigations present rich information about the complex character of the phase transitions. The neutron scattering data⁴³ show the presence of a flat lowest-energy transverse optical branch along q_y direction at $T = 440$ K in the paraelectric phase [see Fig. 6(a)]. This phonon branch is polarized near $[100]$ direction and softens at cooling. The polar soft optical mode, according to the submillimeter spectroscopy data near 10^{12} Hz,⁶² contributes only $\Delta\varepsilon' = 1000$ to the dielectric susceptibility maximum near $T_0 \approx 337$ K [see Fig. 6(b)]. At frequency lowering till 10^7 Hz, the dielectric susceptibility near T_0 rises to $10^4 - 10^5$ [see Fig. 6(c)],⁶³ and at lower frequency obeys the Curie-Weiss law $\varepsilon' = C(T - T_0)^{-1}$

with $C \approx 0.6 \cdot 10^5$ K.

On cooling in the paraelectric phase of $\text{Sn}_2\text{P}_2\text{S}_6$ crystal, not only long wave polarization fluctuations are developed near the Brillouin zone center, which are proportional to the reciprocal of the polar soft optical mode (with B_u symmetry at $q \rightarrow 0$) frequency square. Near the Brillouin zone edge, at $q_y = \pi/b$, also critical growth occurs for fluctuations of atomic motions that are related to the eigenvector of short length phonons from the soft optical branch $B(q_y)$. The development of the aforementioned fluctuations was observed directly [see Fig. 6(d)]⁴⁴ by inelastic X-ray scattering at $T_0 + 2$ K.

The high value of the low frequency dielectric susceptibility on cooling to T_0 is obviously related to crystal lattice anharmonicities. It was earlier supposed^{30,31} that the local three-well potential follows from a nonlinear interaction of polar B_u modes with fully symmetrical A_g modes (like $A_g B_u^2 + A_g^2 B_u^2$) at the Brillouin zone center. But on the matter of the soft optical mode flatness in q_y direction,⁴³ the nonlinear phonon-phonon interaction can be obviously realized with the involvement of phonons from different points of the Brillouin zone. In the simplest approach, such possibility can be incorporated in QAO model^{17,29,35,36} that is based on a three-well on-site potential involving first and second neighbors intersite interactions. Here we consider nonlocal interactions in q_y direction (instead of above considered frustration of J_1 and J_2 inter-site interactions that are related to the incommensurate phase appearance with modulation wave vector q_z). The phase diagram calculated with such model contains a tetracritical point at which two second order transitions lines (from paraelectric into ferroelectric phase and between paraelectric and antipolar phases) intersect. It was found¹⁷ that for $\text{Sn}_2\text{P}_2\text{S}_6$ crystals below T_0 coexistence of antipolar and ferroelectric phases can be presented.

The assumption that in $\text{Sn}_2\text{P}_2\text{S}_6$ crystals the phase transition at $T_0 \approx 337$ K is placed near the tetracritical

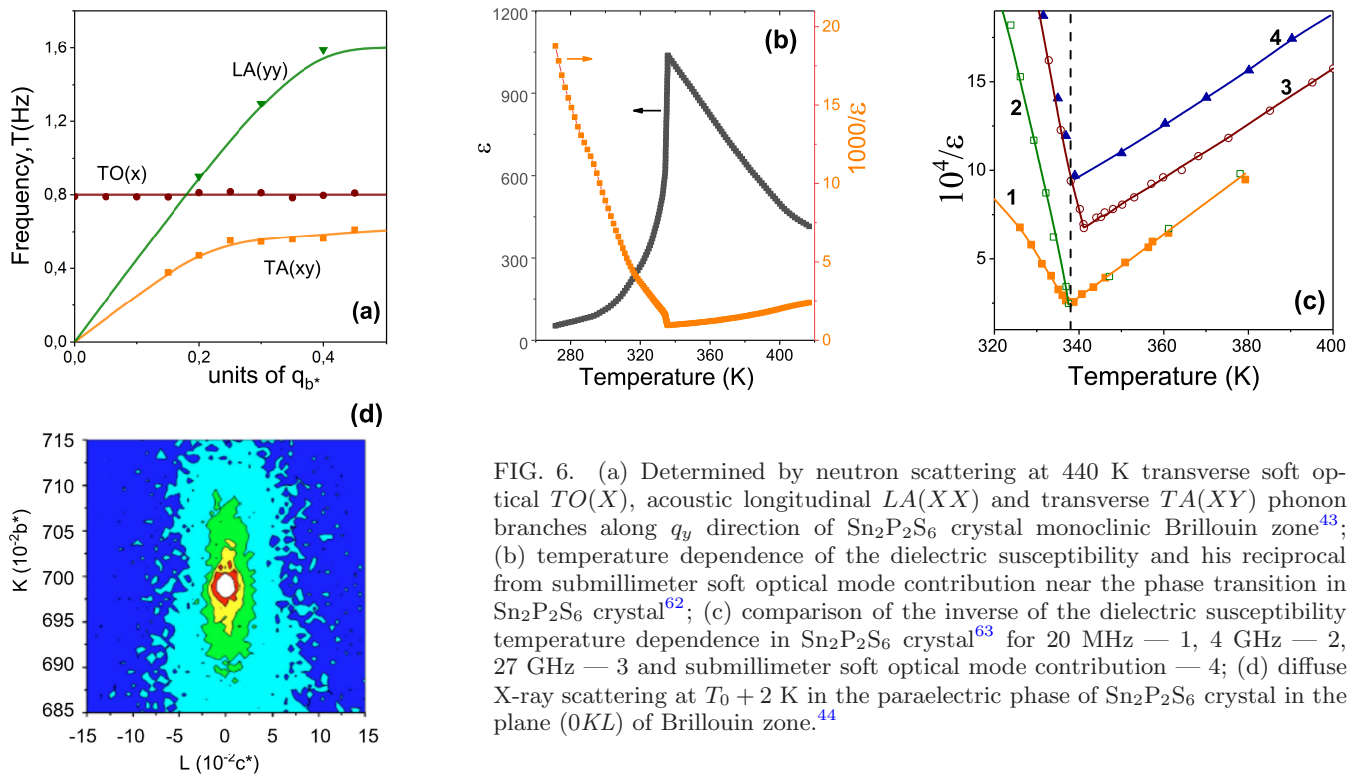


FIG. 6. (a) Determined by neutron scattering at 440 K transverse soft optical $TO(X)$, acoustic longitudinal $LA(XX)$ and transverse $TA(XY)$ phonon branches along q_y direction of $\text{Sn}_2\text{P}_2\text{S}_6$ crystal monoclinic Brillouin zone⁴³; (b) temperature dependence of the dielectric susceptibility and his reciprocal from submillimeter soft optical mode contribution near the phase transition in $\text{Sn}_2\text{P}_2\text{S}_6$ crystal⁶²; (c) comparison of the inverse of the dielectric susceptibility temperature dependence in $\text{Sn}_2\text{P}_2\text{S}_6$ crystal⁶³ for 20 MHz — 1, 4 GHz — 2, 27 GHz — 3 and submillimeter soft optical mode contribution — 4; (d) diffuse X-ray scattering at $T_0 + 2$ K in the paraelectric phase of $\text{Sn}_2\text{P}_2\text{S}_6$ crystal in the plane $(0KL)$ of Brillouin zone.⁴⁴

point agrees with the previous discussion based on the BEG model, for which the phase diagram with a TCP can be complicated by the presence of bicritical or tetracritical points.³⁴ Thus, the critical behavior of $\text{Sn}_2\text{P}_2\text{S}_6$ crystals near temperature T_0 requires special attention.

According to previous investigations of thermal diffusivity,⁵² which is proportional to the reciprocal of heat capacity, the critical behavior of $\text{Sn}_2\text{P}_2\text{S}_6$ can be fitted with a good quality in the paraelectric phase to a model which considers the influence of both fluctuations and defects. On the other hand, below T_0 the best fittings were found using a mean field Landau model. Such asymmetry is very strange, especially when it has been possible to describe the critical behavior of mixed crystals based on $\text{Sn}_2\text{P}_2\text{S}_6$ using a single model for both phases. For $\text{Sn}_2\text{P}_2(\text{Se}_x\text{S}_{1-x})_6$ solutions with increasing selenium concentration and approaching the LP ($x \approx 0.28$), the critical anomalies are nicely described by exponents and ratios of critical amplitudes that belong to the Lifshitz universality class [see Fig. 7(a)].⁵³ At tin by lead substitution in $(\text{Pb}_y\text{Sn}_{1-y})_2\text{P}_2\text{S}_6$ mixed crystals, the critical behavior is also satisfactorily described above and below T_0 as a crossover from a clear non-mean field model at $y = 0.1$ to a mean field one at $y = 0.3$.²⁸ For $\text{Sn}_2\text{P}_2\text{S}_6$ crystals, at the paraelectric to incommensurate second order phase transition the critical anomaly above and below T_i agrees with the predictions of the renormalization group theory for 3D-XY universality class.⁵⁷ At simultaneous substitution of chemical elements in cation and anion sublattices in $(\text{Pb}_y\text{Sn}_{1-y})_2\text{P}_2(\text{Se}_x\text{S}_{1-x})_6$ mixed crystals a TCLP has been found⁵⁰ for $x = 0.28$ and $y = 0.05$

at $T_c = 259.12$ K. Here the tricritical Lifshitz universality class has been assigned by the obtained critical exponent $\alpha = 0.64$ which is equal to the theoretical predicted one.¹¹

Why a critical behavior of $\text{Sn}_2\text{P}_2\text{S}_6$ crystals cant be described satisfactorily in both temperature sides of T_0 ? As was mentioned above, for pure $\text{Sn}_2\text{P}_2\text{S}_6$ crystals below T_0 the coexistence of antipolar (antiferroelectric-like) and ferroelectric states is possible. This is manifested by the observation of double hysteresis loops and usual ferroelectric loops.¹⁷ Considering the possibility of the coexistence of antipolar and ferroelectric phases below T_0 , we reexamine previous experimental data.⁵² We have used for the fittings the well-known equation

$$\frac{1}{D} = B + C\tau + A^\pm |\tau|^{-\alpha} (1 + E^\pm |\tau|^{0.5}), \quad (4)$$

where $\tau = (T - T_0)/T_0$ is the reduced temperature, and superscripts “+” and “-” stand for $T > T_0$ and $T < T_0$, respectively, α , A^\pm , B , C and E^\pm are adjustable parameters. Figure 7(b) demonstrates the fittings together with the deviation plots [see Fig. 7(c)] (difference between each experimental and fitted value, divided by the experimental value, in percentage).

The results of the fittings [see Fig. 7(b),(c)] in $\text{Sn}_2\text{P}_2\text{S}_6$ have shown a XY-like behavior with the critical exponent $\alpha = -0.0092 \pm 0.0008$ below T_0 and Ising like one with $\alpha = 0.1049 \pm 0.0066$ above T_0 . Such value of the critical exponents, smaller than α_{ISING} in the paraelectric phase and a little bigger than α_{XY} below T_0 , can be interpreted as a possible crossover in the critical behavior which ear-

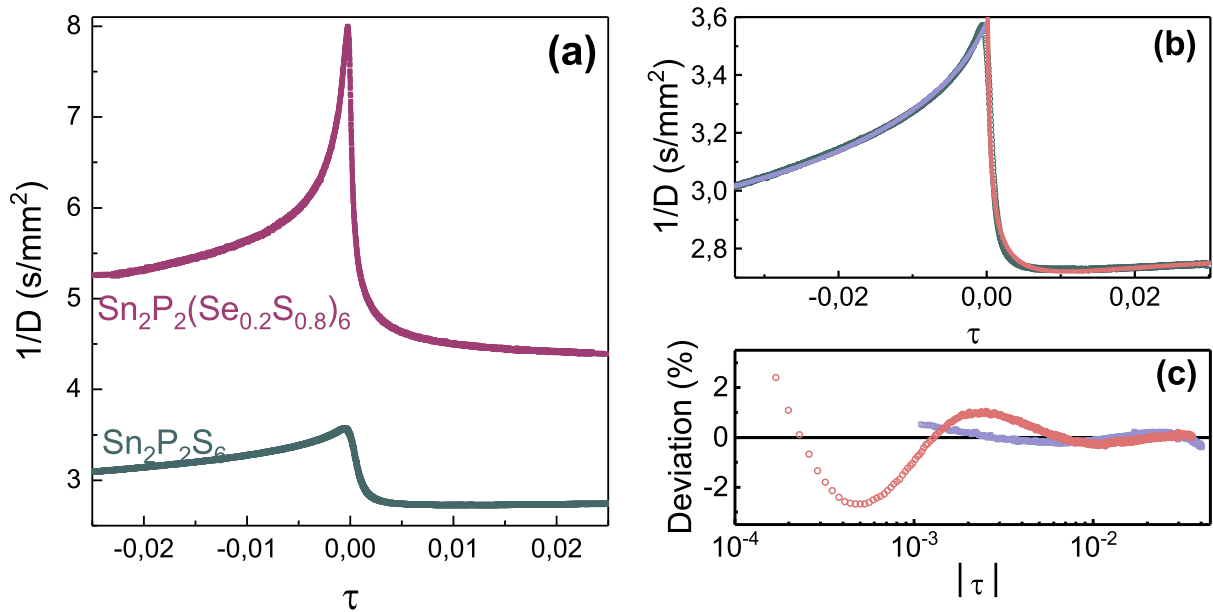


FIG. 7. (a) Dependence of the inverse of thermal diffusivity measured in the [100] crystallographic direction in the vicinity of continuous phase transition in $\text{Sn}_2\text{P}_2\text{S}_6$ and $\text{Sn}_2\text{P}_2(\text{Se}_{0.2}\text{S}_{0.8})_6$ crystals;^{52,53} (b) results of the fittings of the inverse of thermal diffusivity for $\text{Sn}_2\text{P}_2\text{S}_6$ crystal, and (c) corresponding deviation curves for the fittings. The points correspond to experimental measurements, the continuous lines to the fittings to Eq. 4. Blue color corresponds to the fitting below the critical temperature, red to the ones above it.

lier was predicted⁶⁴ for systems with two competing order parameters near a bicritical point on the phase diagram. The bicritical point can be originated instead of a tetracritical point if there is a strong enough coupling of two order parameters.⁶⁵

In any case, good fittings of thermal diffusivity in $\text{Sn}_2\text{P}_2\text{S}_6$ crystal below T_0 with negative value of critical index demonstrate its cups shape that is a characteristic of the antiferroelectric-like ordering and coincides with observed double hysteresis loops in $\text{Sn}_2\text{P}_2\text{S}_6$ crystal below T_0 .¹⁷

IV. CONCLUSIONS

Static and dynamic critical behavior of $\text{Sn}_2\text{P}_2\text{S}_6$ type ferroelectrics and $(\text{Pb}_y\text{Sn}_{1-y})_2\text{P}_2(\text{Se}_x\text{S}_{1-x})_6$ mixed crystals are governed by multicritical points presence on their phase diagram. At hydrostatic compression of $\text{Sn}_2\text{P}_2\text{S}_6$ crystal or at tin by lead substitution in $(\text{Pb}_y\text{Sn}_{1-y})_2\text{P}_2\text{S}_6$ mixed crystals the TCP can be reached, what is described by the BEG model for a system with three-well local potential for pseudospins fluctuations. At sulfur by selenium replacement in $\text{Sn}_2\text{P}_2(\text{Se}_x\text{S}_{1-x})_6$ solid solutions the LP is induced, what is explained by first and second neighbors short range interaction ratio changing in pseudospin ANNNI model. At simultaneous variation of chemical composition in cationic and anionic sublattices the lines of TCPs and LPs on $T - x - y$ phase diagram meet at the TCLP, and this higher order multicritical point can be described in a combined BEG-ANNNI

model.⁴⁵ Below the temperature of TCLP, which can be considered as the Lifshitz line end point, the chaotic state with coexisting ferroelectric and metastable paraelectric and modulated phases is possible. This expectation agrees with the concentration evolution of heat capacity⁵⁷ and dielectric susceptibility⁵⁸ temperature dependence in $(\text{Pb}_y\text{Sn}_{1-y})_2\text{P}_2\text{Se}_6$ mixed crystals, which demonstrates a gradual lock-in transition smearing with growth of lead concentration.

In addition to the frustration of polar fluctuations near the center of the Brillouin zone, in $\text{Sn}_2\text{P}_2\text{S}_6$ crystal the antipolar fluctuations also strongly develop in the paraelectric phase on cooling to the continuous phase transition temperature T_0 . This is confirmed by the observation in neutron scattering experiments⁴³ of a flat polar soft optical phonon branch and by the development of diffuse X-ray scattering along q_y direction in the Brillouin zone of the paraelectric phase near temperature T_0 .⁴⁴ Such observation indicates closeness of this transition to a tetracritical point which appears due to the interaction between two order parameters, related to polar fluctuation near the Brillouin zone center and to antipolar fluctuations near its edge. At strong enough coupling of the mentioned order parameters, the tetracritical point can evolve to a bicritical point. The frequency dependence of the dielectric susceptibility temperature anomaly around T_0 ,^{62,63} together with observed aging effects⁶⁶ and transformation of double hysteresis loops into usual ferroelectric-like loops¹⁷ confirm the possibility of simultaneous development of polar and antipolar fluctuations in the paraelectric phase on cooling to T_0 ,

and the coexistence of antipolar and polar clusters in $\text{Sn}_2\text{P}_2\text{S}_6$ crystals below T_0 . At this transition, the critical behavior according to the thermal diffusivity data⁵² can

be described as a crossover between Ising and XY universality classes, what is expected near a bicritical point with coupled polar and antipolar order parameters.

- ¹ A. D. Bruce and R. A. Cowley, *Structural Phase Transitions* (Taylor and Francis Ltd., London, 1981).
- ² M. E. Lines and A. M. Glass, *Principles and Application of Ferroelectrics and Related Materials* (Clarendon Press, Oxford, 1977).
- ³ R. Blinc and B. Zeks, *Soft Modes in Ferroelectrics and Antiferroelectrics* (North-Holland, Amsterdam, 1974).
- ⁴ A. Y. Borisevich, E. A. Eliseev, A. N. Morozovska, C.-J. Cheng, J.-Y. Lin, Y. H. Chu, D. Kan, I. Takeuchi, V. Nagarajan, and S. V. Kalinin, *Nat. Commun.* **3**, 775 (2012).
- ⁵ E. V. Balashova and A. K. Tagantsev, *Phys. Rev. B* **48**, 9979 (1993).
- ⁶ A. K. Tagantsev, K. Vaideeswaran, S. B. Vakhru-shev, A. V. Filimonov, R. G. Burkovsky, A. Shaganov, D. Andronikova, A. I. Rudskoy, A. Q. R. Baron, H. Uchiyama, D. Chernyshov, A. Bosak, Z. Ujma, K. Roleder, A. Majchrowski, J.-H. Ko, and N. Setter, *Nat. Commun.* **4**, 2229 (2013).
- ⁷ J. Hlinka, T. Ostapchuk, E. Buixaderas, C. Kadlec, P. Kuzel, I. Gregora, J. Kroupa, M. Savinov, A. Klic, J. Drahekoupil, I. Etxebarria, and J. Dec, *Phys. Rev. Lett.* **112**, 197601-1 (2014).
- ⁸ Yu. M. Vysochanskii, M. M. Mayor, V. M. Rizak, V. Yu. Slivka, and M. M. Khoma, *JETP* **68**, 782 (1989).
- ⁹ Yu. M. Vysochanskii and V. Yu. Slivka, *Sov. Phys. Usp.* **35**, 123 (1992).
- ¹⁰ R. Folk and G. Moser, *Phys. Rev. B* **47**, 13992 (1993).
- ¹¹ R. Folk, *Phase Transitions* **67**, 645 (1999).
- ¹² Alexander A. Grabar, Yulian M. Vysochanskii, Alexander N. Shumelyuk, Mojca Jazbinsek, Germano Montemezzani, and Peter Gunter, in *Photorefractive Materials and Their Applications*, edited by P. Gunter and J.P. Huignard (Springer Verlag, Heidelberg, 2006).
- ¹³ Y. W. Cho, S. K. Choi, and Yu. M. Vysochanskii, *J. Mater. Res.* **16**, 3317 (2001).
- ¹⁴ S. Huang, C. Meng, M. Xiao, S. Ren, Sh. Wang, D. Han, Yu. Li, and Yu. Meng, *Small* **14**, 1704367 (2018).
- ¹⁵ F. C. Penning, M. M. Maior, S. A. J. Wieggers, H. van Kempen, and J. C. Maan, *Rev. Sci. Instrum.* **67**, 2602 (1996).
- ¹⁶ M. M. Major, Sh. B. Molnar, Yu. M. Vysochanskii, M. I. Gurzan, P. H. M. van Loosdrecht, P. J. E. M. van der Linden, and H. van Kempen, *Appl. Phys. Lett.* **62**, 2646 (1993).
- ¹⁷ I. Zamaraita, R. Yevych, A. Dziaugys, A. Molnar, J. Banys, S. Svirskas, and Yu. Vysochanskii, *Phys. Rev. Appl.* **10**, 034017-1 (2018).
- ¹⁸ S. Grubel, J. A. Johnson, P. Beaud, C. Dornes, A. Ferrer, V. Haborets, L. Huber, T. Huber, A. Kohutych, T. Kubacka, M. Kubli, S. O. Mariager, J. Rittmann, J. I. Saari, Y. Vysochanskii, G. Ingold, and S. L. Johnson, [arXiv:1602.05435 \[cond-mat.mtrl-sci\]](https://arxiv.org/abs/1602.05435) (2016).
- ¹⁹ E. A. Eliseev, Ye. M. Fomichov, S. V. Kalinin, Yu. M. Vysochanskii, P. Maksymovich, and A. N. Morozovska, *Phys. Rev. B* **98**, 054101-1 (2018).
- ²⁰ A. N. Morozovska, Eu. A. Eliseev, Ye. M. Fomichov, Yu. M. Vysochanskii, V. Yu. Reshetnyak, and D. R. Evans, *Acta Mater.* **183**, 36 (2020).
- ²¹ A. N. Rubtsov, J. Hlinka, and T. Janssen, *Phys. Rev. E* **61**, 126 (2000).
- ²² J. Hlinka, T. Janssen, and V. Dvořák, *J. Phys.: Condens. Matter* **11**, 3209 (1999).
- ²³ K. Moriya, H. Kuniyoshi, K. Tashita, Y. Ozaki, S. Yano, and T. Matsuo, *J. Phys. Soc. Jpn.* **67**, 3505 (1998).
- ²⁴ Yu. M. Vysochanskii, T. Janssen, R. Currat, R. Folk, J. Banys, J. Grigas, V. Samulionis, *Phase transitions in ferroelectric phosphorous chalcogenide crystals* (Vilnius University Publishing House, 2006).
- ²⁵ P. Ondrejko, M. Kempa, Y. Vysochanskii, P. Saint-Gregoire, P. Bourges, K. Rushchanskii, and J. Hlinka, *Phys. Rev. B* **86**, 224106-1 (2012).
- ²⁶ P. Ondrejko, M. Guennou, M. Kempa, Y. Vysochanskii, G. Garbarino, and J. Hlinka, *J. Phys.: Condens. Matter* **25**, 115901 (2013).
- ²⁷ K. Z. Rushchanskii, R. M. Bilanych, A. A. Molnar, R. M. Yevych, A. A. Kohutych, S. I. Perechinskii, V. Samulionis, J. Banys, and Y. M. Vysochanskii, *Phys. Status Solidi B* **253**, 384 (2016).
- ²⁸ V. Shvalya, A. Oleaga, A. Salazar, A. A. Kohutych, and Yu. M. Vysochanskii, *Thermochim. Acta* **617**, 136 (2015).
- ²⁹ R. Yevych, V. Haborets, M. Medulych, A. Molnar, A. Kohutych, A. Dziaugys, Ju. Banys, and Yu. Vysochanskii, *Low Temperature Physics* **42**, 1155 (2016).
- ³⁰ K. Z. Rushchanskii, Yu. M. Vysochanskii, and D. Strauch, *Phys. Rev. Lett.* **99**, 207601-1 (2007).
- ³¹ K. Glukhov, K. Fedyo, J. Banys, and Yu. Vysochanskii, *Int. J. Mol. Sci.* **13**, 14356 (2012).
- ³² X. Bourdon, A. Grimmer, A. Kretschmer, and V. Cajipe, in *Proceedings of the 30th Congress Ampere on Magnetic Resonance and Related Phenomena*, Lisbon, Portugal, 2328 July 2000.
- ³³ M. Blume, V. J. Emery, and R. B. Griffiths, *Phys. Rev. A* **4**, 1071 (1971).
- ³⁴ W. Hoston and A. N. Berker, *Phys. Rev. Lett.* **67**, 1027 (1991).
- ³⁵ R. Yevych, M. Medulych, and Yu. Vysochanskii, *Condens. Matter Phys.* **21**, 23001-1 (2018).
- ³⁶ R. Yevych and Yu. Vysochanskii, *Condens. Matter Phys.* **21**, 33001-1 (2018).
- ³⁷ W. Selke, *Physics Reports* **170**, 213 (1988).
- ³⁸ S. W. H. Eijt, R. Currat, J. E. Lorenzo, P. Saint-Gregoire, S. Katano, T. Janssen, B. Hennion, and Yu. M. Vysochanskii, *J. Phys.: Cond. Matt.* **10**, 4811 (1998).
- ³⁹ A. Kohutych, R. Yevych, S. Perechinskii, V. Samulionis, J. Banys, and Yu. Vysochanskii, *Phys. Rev. B* **82**, 054101-1 (2010).
- ⁴⁰ A. N. Morozovska, Yu. M. Vysochanskii, O. V. Varenyk, M. V. Silibin, S. V. Kalinin, and Eu. A. Eliseev, *Phys. Rev. B* **92**, 094308-1 (2015).
- ⁴¹ A. N. Morozovska, M. D. Glinchuk, Eu. A. Eliseev, and Yu. M. Vysochanskii, *Phys. Rev. B* **96**, 094111-1 (2017).
- ⁴² R. M. Yevych, Yu. M. Vysochanskii, M. M. Khoma, and S. I. Perechinskii,

- J. Phys.: Condens. Matter* **18**, 4047 (2006).
- ⁴³ S. W.H. Eijt, R. Currat, J. E. Lorenzo, P. Saint-Grgoire, B. Hennion, and Yu. M. Vysochanskii, *Eur. Phys. J. B* **5**, 169 (1998).
- ⁴⁴ J. Hlinka, R. Currat, M. de Boissieu, F. Livet, and Yu. M. Vysochanskii, *Phys. Rev. B* **71**, 052102 (2005).
- ⁴⁵ T. Tome and S.R. Salinas, *Phys. Rev. A* **39**, 2206 (1989).
- ⁴⁶ P. J. Jensen, K. A. Penson and K. H. Bennemann, *Phys. Rev. B* **35**, 7306 (1987).
- ⁴⁷ A. Aharony, E. Domany, R. M. Hornreich, T. Schneider, and M. Zannetti, *Phys. Rev. B* **32**, 3358 (1985).
- ⁴⁸ N. S. Tonchev and D. I. Uzunov, *Physica A* **134**, 265 (1985).
- ⁴⁹ Afaf Abdel-Hady and R. Folk, *Phys. Rev. B* **54**, 3851 (1996).
- ⁵⁰ A. Oleaga, V. Shvalya, A. Salazar, I. Stoika, and Yu. M. Vysochanskii, *J. Alloys Compd.* **694**, 808 (2017).
- ⁵¹ T. M. Rice and L. Sheddou, *Phys. Rev. Lett.* **47**, 689 (1981).
- ⁵² A. Oleaga, A. Salazar, M. Massot, and Yu. M. Vysochanskii, *Termochim. Acta* **459**, 73 (2007).
- ⁵³ A. Oleaga, A. Salazar, A. A. Kohutysh, Yu. M. Vysochanskii, *J. Phys.: Condens. Matter* **23**, 025902-1 (2011).
- ⁵⁴ V. Shvalya, A. Oleaga, A. Salazar, I. Stoika, and Yu. M. Vysochanskii, *J. Mater. Sci.* **51**, 8156 (2016).
- ⁵⁵ V. Shvalya, A. Oleaga, A. Salazar, A. A. Kohutysh, and Yu. M. Vysochanskii, *J. Phys. Chem. Solids* **88**, 78 (2016).
- ⁵⁶ A. Oleaga, V. Liubachko, A. Salazar, and Yu. Vysochanskii, *Termochim. Acta* **675**, 38 (2019).
- ⁵⁷ K. Moriya, T. Yamada, K. Saka, S. Yano, S. Baluya, T. Matsuo, P. Pritz, and Yu. Vysochanskii, *J. Therm. Anal. Calorim.* **70**, 321 (2002).
- ⁵⁸ Yu. M. Vysochanskii, M. M. Maior, V. Yu. Slivka, and M. I. Gurzan, *Fiz. Tverd. Tela* **27**, 1560 (1985) [in Russian].
- ⁵⁹ V. Yu. Korda, S. V. Berezovsky, A. S. Molev, L. P. Korda, and V. F. Klepikov, *Physica B* **407**, 3388 (2012).
- ⁶⁰ V. Yu. Korda, S. V. Berezovsky, A. S. Molev, L. P. Korda, and V. F. Klepikov, *Physica B* **425**, 31 (2013).
- ⁶¹ G. H. F. van Raaij, K. J. H. van Bommel, and T. Janssen, *Phys. Rev. B* **62**, 3751 (2000).
- ⁶² A. A. Volkov, G. V. Kozlov, N. I. Afanasjeva, A. A. Grabar, Yu. M. Vysochanskii, and V. Yu. Slivka, *Fiz. Tverd. Tela* **25**, 2575 (1983) [in Russian].
- ⁶³ J. Grigas, *Ferroelectrics* **380**, 113 (2009).
- ⁶⁴ J. M. Kosterlitz, D. R. Nelson, and M. E. Fishert, *Phys. Rev. B* **13**, 412 (1976).
- ⁶⁵ R. Folk, Yu. Holovatch, and G. Moser, *Phys. Rev. E* **78**, 041124 (2008).
- ⁶⁶ A. A. Molnar, Yu. M. Vysochanskii, A. A. Gorvat, and Yu. S. Nakonechnii, *Ferroelectrics* **174**, 41 (1995).